Energetics of domain formation in thermomagnetic recording

Cite as: Journal of Applied Physics **55**, 3049 (1984); https://doi.org/10.1063/1.333298
Submitted: 26 September 1983 . Accepted: 14 November 1983 . Published Online: 04 June 1998

M. Mansuripur, and G. A. N. Connell

Energetics of domain formation in thermomagnetic recording

M. Mansuripur
College of Engineering, Boston University, Boston, Massachusetts 02215

G. A. N. Connell
Xerox Palo Alto Research Center, Palo Alto, California 94304

(Received 26 September 1983; accepted for publication 14 November 1983)

A new model for the distribution of perpendicular magnetization in thin magnetic films supporting a circular domain is proposed. The contributions of various sources to the magnetic energy are determined and the demagnetizing effect in particular is discussed at length. It is shown that a demagnetizing energy density per unit area of the domain wall can be defined which, unlike the domain wall energy density arising from exchange and anisotropy contributions, is a function of film thickness h. For domains of large radius and small wall thickness (compared with h), the demagnetizing energy density is found to be linearly increasing with h. A typical cycle of thermomagnetic recording on a thin ferrimagnetic film with room temperature compensation point is then studied, and the effect of various parameters on the formation process and stability of reverse magnetized domains is discussed.

PACS numbers: 75.70.Kw, 85.70.Kh, 75.30.Cr, 75.50.Gy

I. INTRODUCTION

The process of thermomagnetic recording involves the formation of a reverse magnetized domain in the region of the hot spot produced by a focussed laser beam on a perpendicularly magnetized medium and the subsequent growth or contraction of this domain as the heating and then cooling progresses. The behavior of the spin system under conditions of thermomagnetic writing is a complicated process which is not completely understood at the present time. Nevertheless, it is possible to investigate the problem phenomenologically by the consideration of magnetic energy and the notion of coercivity.[1] A necessary ingredient of such a study is the calculation of the different contributions to the energy, assessment of their relative significance, and tracking of the net energy variations over a cycle of thermomagnetic recording. In this paper, we report some preliminary results of our study of the energetics of domain formation during a full cycle of thermomagnetic recording. These results provide insight into the nature of forces that act on the domain walls and serve as a guide to help us quantify the wall coercivities that are required for the recording of spots with various characteristics.

Section II describes the function that has been used in our calculations to represent the magnetization of a circular domain. In Sec. III, we derive expressions for various contributions to the magnetic energy of a thin film in the presence of a reverse magnetized domain and discuss some interesting features of the demagnetizing energy. Section IV describes the numerical results obtained for a quadrilayer disk storage medium that has been shown to have superior optical and thermal properties for magnetooptical storage of information.[2,3] Some final remarks are made in Sec. V.

II. DISTRIBUTION OF MAGNETIZATION IN PERPENDICULARLY MAGNETIZED THIN FILMS SUPPORTING A SATURATED CIRCULAR DOMAIN

In a perpendicularly magnetized film, straight domain walls of Bloch type are known to obey the following relationship[4]:

$$\cos[\varphi(x)] = \tanh\left(\frac{x - x_0}{\lambda_0}\right). \tag{1}$$

Here the film is assumed to lie in the XY plane with the domain wall parallel to the Y axis and centered at $X = X_0$. $\varphi(X)$ is the angle between the magnetization vector $M(X)$ and the Z axis, and $\lambda_0 = (A/K_u)^{1/2}$ is the domain wall parameter, with A being the exchange constant and K_u representing the anisotropy energy density. The domain wall thickness is proportional to λ_0 and the proportionality constant is usually taken to be 4 (i.e., $4\lambda_0$ is the domain wall thickness).

When one considers a circular domain such as the one in Fig. 1, it might seem reasonable to assume the same kind of relationship for the deviation of magnetization from normal, i.e.,

$$\cos[\varphi(r)] = \tanh\left(\frac{r - r_0}{\lambda}\right), \tag{2}$$

where now r is the distance from the center of the domain and r_0 is the location of the domain wall. In particular, when

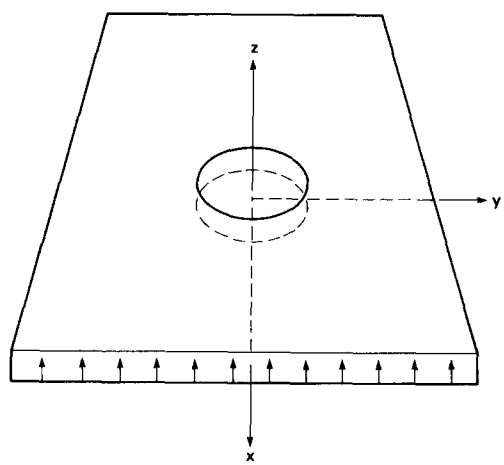

FIG. 1. Schematic representation of a circular domain in a perpendicularly magnetized film.

 0021-8979/84/083049-07$02.40

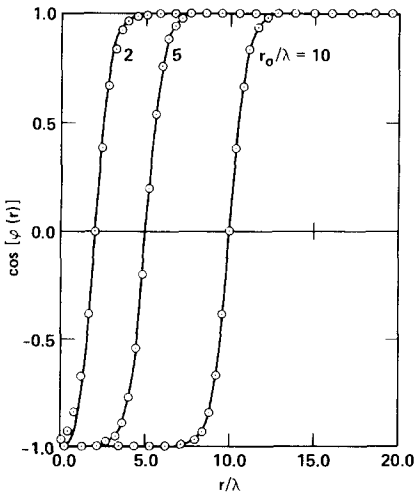

FIG. 2. Plots of Eq. (3) (solid curve) and Eq. (2) (O O O) vs r/λ for several values of r_0/λ.

$r_0 \gg \lambda$ the curvature of the wall becomes negligible and the model accurately describes the situation. The problem with this model is that the exchange energy at the center of the domain ($r = 0$) becomes infinitely large, and one has to truncate the function in the neighborhood of $r = 0$ in order to obtain reasonable results. To avoid this problem, we have assumed a slightly different model, namely,

$$\cos[\varphi(r)] = \tanh\left(\frac{r^3 - r_0^3}{3\lambda r r_0}\right). \tag{3}$$

The above function approximates Eq. (2) very closely when $r_0 \gg \lambda$ and yet its asymptotic approach to $r = 0$ eliminates the problem with exchange energy. Figure 2 shows plots of $\cos[\varphi(r)]$ vs (r/λ) for various values of (r_0/λ). The solid lines represent Eq. (3) while the dots represent Eq. (2). Notice that when $(r_0/\lambda) \geqslant 5$, the two equations are extremely similar. For smaller values of (r_0/λ) the two equations differ mainly in the tails of the transition region. It is this difference in the neighborhood of $r = 0$ that makes Eq. (3) an appropriate model of domain magnetization. We must emphasize that Eq. (3) is not the analytical solution to the variational problem of minimization of the domain wall energy of a cylindrical domain, a problem that leads to an as yet intractable non-linear differential equation. It is a simple function, however, that has the correct asymptotic properties and can be thought of as a parametric representation of domain magnetization with r_0 being the domain radius. The parameter λ is no longer solely determined by $(A/K_u)^{1/2}$; instead, it is determined numerically to minimize the total energy of the domain. Equation (3) has the property that when the domain radius is large enough for the effects of domain wall curvature to be negligible, it approaches the equation for straight domain walls [Eq. (1)].

In the next section we use Eq. (3) as the model for domain magnetization to obtain various contributions to energy due to the existence of a circular domain.

III. ENERGETICS OF DOMAIN FORMATION

There are four major contributors to the energy of a reverse magnetized domain: external field energy, anisotropy energy, exchange energy, and self (demagnetizing) energy.[5] In this section we calculate the contributions of each of these sources to the total energy when a domain of radius r_0 and wall parameter λ is created in a film of thickness h. The initial magnetization is assumed to be uniform throughout the film thickness with perpendicular orientation and to have circular symmetry in the plane of the film, namely $M(r,\theta,z) \equiv M(r)$. The presence of a circular domain will then change the distribution according to the following relationships:

$$\begin{aligned} M_x(r,\theta) &= -M(r)\sin[\varphi(r)]\sin\theta, \\ M_y(r,\theta) &= M(r)\sin[\varphi(r)]\cos\theta, \\ M_z(r) &= M(r)\cos[\varphi(r)]. \end{aligned} \tag{4}$$

The function $\varphi(r)$ in the above equations is given by Eq. (3). We now proceed to calculate the contributions to energy from the aforementioned sources.

A. External field energy

Assuming that a uniform field H is applied in the Z direction, the energy in the absence of the domain is given by

$$E_H = -\int_0^\infty 2\pi r h H\, M(r)\, dr. \tag{5}$$

In the presence of the domain the energy will be

$$E_H = -\int_0^\infty 2\pi r h\, H\, M(r)\cos[\varphi(r)]\, dr. \tag{6}$$

The energy difference is therefore given by

$$\Delta E_H = 2\pi h H \int_0^\infty M(r) f_H(r)\, dr, \tag{7}$$

where

$$f_H(r) = r\left[1 - \tanh\left(\frac{r^3 - r_0^3}{3\lambda r r_0}\right)\right].$$

Figure 3 shows plots of the function $f_H(r)$ vs r/λ for various values of r_0/λ. When $M(r) = M_s = \text{const.}$ and $r_0/\lambda \gg 1$ the above equation closely approximates the well-known relation $\Delta E_H = 2\pi r_0^2 h H M_s$.

B. Anisotropy energy

In the presence of uniaxial anisotropy in the perpendicular direction, the deviation of magnetization vector from

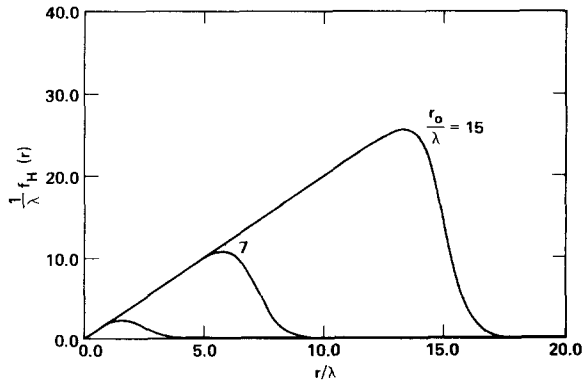

FIG. 3. Normalized plot of $f_H(r)$ vs r/λ for several values at r_0/λ.

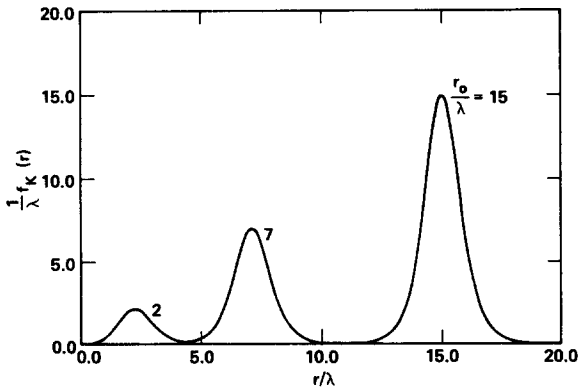

FIG. 4. Normalized plot of $f_K(r)$ vs r/λ for several values of r_0/λ.

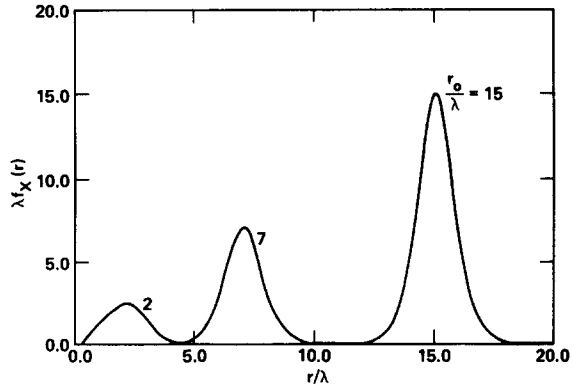

FIG. 5. Normalized plot of $f_x(r)$ vs r/λ for several values of r_0/λ.

the Z axis gives rise to an additional energy term, known as the anisotropy energy. Assuming that the anisotropy energy density constant is $K_u(r)$, the increase is given by

$$\Delta E_K = \int_0^\infty 2\pi r\ hK_u(r)\sin^2[\varphi(r)]\,dr$$

$$= 2\pi h\int_0^\infty K_u(r) f_K(r)\,dr, \tag{8}$$

where

$$f_K(r) = r\left[1 - \tanh^2\left(\frac{r^3 - r_0^3}{3\lambda r r_0}\right)\right].$$

The function $f_K(r)$ is plotted in Fig. 4 versus (r/λ) for various values of (r_0/λ). When $K_u(r) = K_u = \text{const.}$ and $r_0 \gg \lambda$, Eq. (8) closely approximates the relation $\Delta E_K = 4\pi K_u r_0 h\lambda$ which would have been obtained if curvature of the wall had been neglected.

C. Exchange energy

The appearance of a domain in a magnetic medium is accompanied by an increase in the free energy, which on a microscopic scale can be described in terms of the variation in the direction of magnetization across the plane of the film. The energy difference can be expressed by the following relation:

$$\Delta E_x = \int_0^\infty 2\pi r h A(r)[(\nabla\alpha)^2 + (\nabla\beta)^2 + (\nabla\gamma)^2]\,dr, \tag{9}$$

in which

$$\alpha(r,\theta) = \sin[\varphi(r)]\sin\theta,$$

$$\beta(r,\theta) = \sin[\varphi(r)]\cos\theta,$$

$$\gamma(r) = \cos[\varphi(r)]$$

are the direction cosines of the magnetization vector, and

$$\nabla = \frac{\partial}{\partial r}\hat{a}_r + \frac{1}{r}\frac{\partial}{\partial\theta}\hat{a}_\theta + \frac{\partial}{\partial z}\hat{a}_z$$

is the gradient operator in the cylindrical coordinates. $A(r)$ is the exchange stiffness constant. After algebraic manipulations, Eq. (9) reduces to

$$\Delta E_x = 2\pi h\int_0^\infty A(r) f_x(r)\,dr, \tag{10}$$

where

$$f_x(r) = \frac{1}{r}\left[1 + \left(\frac{2r^3 + r_0^3}{3\lambda r r_0}\right)^2\right]\left[1 - \tanh^2\left(\frac{r^3 - r_0^3}{3\lambda r r_0}\right)\right].$$

The function $f_x(r)$ is plotted versus r/λ for several values of r_0/λ in Fig. 5. Notice that the function approaches zero as $r \to 0$ for all values of r_0. This property is due to the asymptotic behavior of the function $\tanh[(r^3 - r_0^3)/3rr_0]$ around $r = 0$ and is the reason why Eq.(3) was chosen to represent the domain rather than Eq. (2). When $A(r) = A = \text{const.}$ and $r_0 \gg \lambda$, Eq. (10) closely approximates the relation $\Delta E_x = 4\pi A r_0 h/\lambda$, which would have been obtained if curvature of the wall had been neglected.

D. Self (demagnetizing) energy

The general expression for the demagnetizing energy E_M is the following[6]:

$$E_M = \frac{1}{2}\int_V\int_{V'}\frac{(\nabla\cdot M)(\nabla\cdot M')}{|r - r'|}\,dV\,dV', \tag{11}$$

where V is the region of space that contains the magnetic material and $|r - r'| = [r^2 + r'^2 - 2rr'\cos(\theta - \theta') + (z - z')^2]^{1/2}$ is the distance between points located at r and r'. In cylindrical coordinates, the divergence operator is given by

$$\nabla\cdot A = \frac{1}{r}\frac{\partial}{\partial r}(rA_r) + \frac{1}{r}\frac{\partial}{\partial_\theta}(A_\theta) + \frac{\partial}{\partial z}(A_z). \tag{12}$$

For a thin film of thickness h, having perpendicular magnetization distributed with circular symmetry, we have

$$M(r,\theta,z) = M(r)\{\sin[\varphi(r)]\,\hat{a}_\theta + \cos[\varphi(r)]\,\hat{a}_z\}$$

$$\times[U(z) - U(z - h)]. \tag{13}$$

Here $U(z)$ is the unit step function and $M(r)$ is the magnitude of saturation magnetization at radius r. For this distribution, the divergence is given by

$$\nabla\cdot M = M(r)\cos[\varphi(r)][\delta(z) - \delta(z - h)], \tag{14}$$

where $\delta(z)$ is the Dirac delta function. Equation (14) can now be used in Eq. (11) to yield the demagnetizing energy. After some algebraic manipulations, we arrive at

$$E_M = 16\pi\int_{r=0}^\infty\int_{r'=0}^r M(r)M(r')\cos[\varphi(r)]$$

$$\times\cos[\varphi(r')]\left[r'K(r'/r) - \frac{rr'}{\sqrt{(r + r')^2 + h^2}}\right.$$

$$\left.\times K\left(\sqrt{\frac{4rr'}{(r + r')^2 + h^2}}\right)\right]dr\,dr', \tag{15}$$

where

$$K(\chi)=\int_0^{\pi/2}(1-\chi^2\sin^2\theta)^{-1/2}\,d\theta$$

is the complete elliptic integral of the first kind.

Before proceeding further, let us examine the behavior of different functions that appear in Eq. (15). For simplicity, we consider the case where the magnetization distribution is uniform, i.e., $M(r)=M_s=\text{const}$. Then

$$E_M=(2\pi M_s^2)\int_{r=0}^{\infty}2\pi rh\int_{r'=0}^{r}\cos[\varphi(r)]\times\cos[\varphi(r')]\,g(r,r',h)\,dr'\,dr, \tag{16}$$

where

$$g(r,r',h)=\frac{4}{\pi h}\left[\frac{r'}{r}K\left(\frac{r'}{r}\right)-\frac{r'}{\sqrt{(r+r')^2+h^2}}K\left(\sqrt{\frac{4rr'}{(r+r')^2+h^2}}\right)\right]. \tag{17}$$

In the absence of reverse magnetized domains, $\cos[\varphi(r)]=\cos[\varphi(r')]=1$ and the inner integral in Eq. (16) can be written as

$$\int_{r'=0}^{r}g(r,r',h)\,dr'=\frac{4r}{\pi h}\int_0^1\left[K(x)-\frac{K\left(\sqrt{\frac{4x}{(1+x)^2+(h/r)^2}}\right)}{\sqrt{(1+x)^2+(h/r)^2}}\right]x\,dx=f(r/h). \tag{18}$$

A plot of the function $f(r/h)$ is shown in Fig. 6; notice that the function approaches unity for $r\gg h$. The demagnetizing energy for a magnetic disk of radius R and thickness h, magnetized to M_s in the axial direction is now

$$E_M=(2\pi M_s^2)\int_{r=0}^{R}2\pi rhf(r/h)\,dr, \tag{19}$$

and as $R\to\infty$ the energy density approaches $2\pi M_s^2$.

When a magnetic domain is present, $\cos[\varphi(r)]$ is given by Eq. (3) and upon normalization of parameters, the inner integral in Eq.(16) becomes

$$\left(\frac{4\rho}{\pi}\right)\tanh\left(\frac{\rho^3-\rho_0^3}{3\Lambda\rho\rho_0}\right)\int_0^1\tanh\left(\frac{(\rho x)^3-\rho_0^3}{3\Lambda\rho\rho_0 x}\right)\left[K(x)-\frac{K\left(\sqrt{\frac{4x}{(1+x)^2+\rho^{-2}}}\right)}{\sqrt{(1+x)^2+\rho^{-2}}}\right]x\,dx=F(\rho,\rho_0,\Lambda). \tag{20}$$

In the above expression, $\rho=r/h,\rho_0/h$, and $\Lambda=\lambda/h$ are the normalized parameters with respect to be film thickness. Figure 7 is a plot of $F(\rho,\rho_0,\Lambda)$ versus ρ for $\rho_0=35$ and $\Lambda=1$. Since the demagnetizing energy is now expressed as

$$E_M=(2\pi M_s^2)\int_{r=0}^{\infty}2\pi rh\;F(r/h,r_0/h,\lambda/h)\,dr, \tag{21}$$

it can be seen from Fig. 7 that the presence of a domain wall at r_0 reduces the demagnetizing energy at and around $r=r_0$. The reduction is due to the reduced demagnetizing field and nonperpendicular magnetization in the region of the domain wall. The fact that the curve in Fig. 7 is negative in a small region around $r=r_0$ may indicate that the demagnetizing field in this region has the same direction as the magnetization, although it might also be an artifact of the assumed form of the wall profile.

Qualitatively, the behavior of $F(\rho,\rho_0,\Lambda)$ for various values of ρ_0 and Λ remains the same. The increasing of Λ, however, makes the notch around ρ_0 wider while decreasing of Λ has the opposite effect. This is in agreement with the intuitive suggestion that a thick domain wall should reduce the demagnetizing energy more than a thin domain wall.

The reduction in self magnetic energy, caused by the creation of a circular domain of radius r_0 and wall parameter λ, can now be obtained by subtracting Eq. (21) from Eq. (19), namely

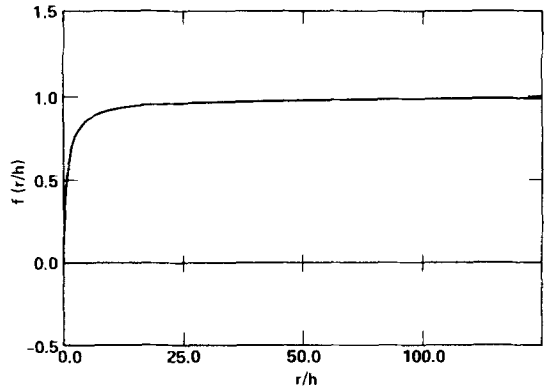

FIG. 6. Plot of $f(r/h)$ vs r/h.

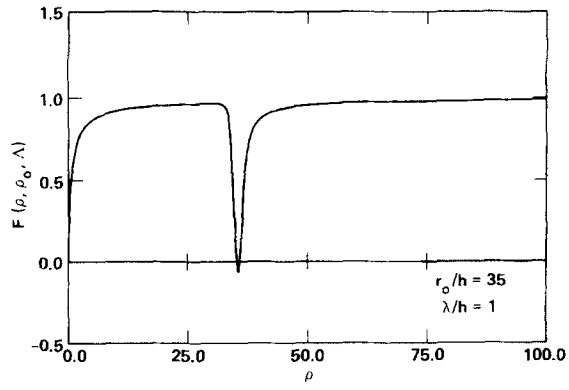

FIG. 7. Plot of $F(\rho,\rho_0,\Lambda)$ vs ρ for $\rho_0=35$ and $\Lambda=1$.

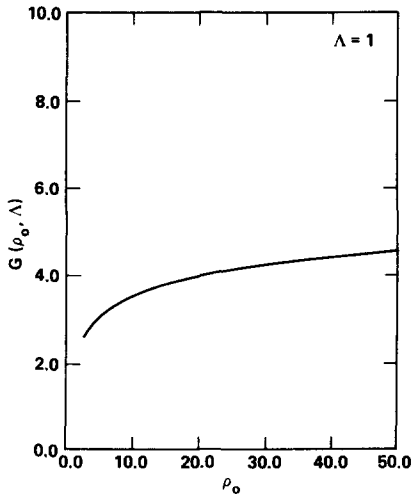

FIG. 8. Plot of $G(\rho_0,\Lambda)$ vs ρ_0 for $\Lambda = 1$.

$$\Delta E_M = (2\pi M_s^2)\int_0^\infty 2\pi rh \times [f(r/h) - F(r/h, r_0/h, \lambda/h)]\, dr = (2\pi M_s^2)(2\pi r_0 h^2)\, G(r_0/h, \lambda/h), \quad (22)$$

where

$$G(\rho_0,\Lambda) = \int_0^\infty (\rho/\rho_0)[f(\rho) - F(\rho, \rho_0\Lambda)]\, d\rho. \quad (23)$$

Figure 8 shows a plot of $G(\rho_0,\Lambda)$ vs ρ_0 for $\Lambda = 1$. Notice that the function is relatively constant for large ρ_0, indicating that the curvature of the wall has no significant effect on the demagnetizing energy of large domains. The value of this constant is a function of Λ. Figure 9 shows a plot of $G(\rho_0,\Lambda)$ vs Λ for $\rho_0 = 20$. As Λ approaches zero, the function approaches a constant value (~ 3). For a thin domain wall of large radius (both compared to the film thickness) therefore, a good estimate of self magnetic energy per unit area of domain wall is given by $\Delta E_M/2\pi r_0 h \approx 6\pi h M_s^2$. This quantity should be compared with the domain wall energy density ($\sigma_w = 4\sqrt{AK_u}$) to determine whether the reduction in self-magnetic energy alone can compensate for the creation of a domain wall.

IV. AN EXAMPLE OF THERMOMAGNETIC RECORDING PROCESS

We now use the results of the previous section to calculate the variations of total magnetic energy in a thin ferrimagnetic film during a typical thermomagnetic recording cycle. The film is incorporated in a quadrilayer structure as shown in Fig. 10 and illumination is achieved by a $5^{mW} - 50^{nS}$ pulse from an infrared laser (wavelength = 840 nm), focussed to a Gaussian spot of 1 μm diam at the e^{-1} point. The distribution of temperature in the magnetic film is calculated numerically[7] and shown in Fig. 11. It is assumed that an external magnetic field $H_{ext} = 400$ Oe is applied opposite to the direction of magnetization to help form the domain.

The following procedure is used for the calculations of this section: At a given instant of time t we calculate the temperature distribution in the magnetic film as a function of distance r from the center of the beam and, using a mean-field approximation[8,9] for the saturation magnetization M_s, determine the distributions $M_s(r)$, $A(r)$, and $K_u(r)$, where A and K_u are the temperature-dependent exchange stiffness and anisotropy energy parameters respectively. The temperature dependence of K_u is assumed to obey a simple second order relation with the sublattice magnetizations M_1 and M_2, namely $K_u = (|M_1| + |M_2|)^2$, which is a reasonable assumption, considering the arguments of Mizoguchi *et al.*[10] Moreover, it turns out that our qualitative results are insensitive to the specific values of K_u as long as its general behavior as a function of temperature remains the same. We then assume the existence of a domain of radius r_0 and wall thickness parameter λ and calculate the total energy of the domain $E_T(r_0, \lambda)$ vs λ. E_T can be minimized with respect to λ to give the net energy $E_T(r_0)$ of the domain at time t.

Figure 12 shows the temperature dependence of M_s, A, and K_u for a ferrimagnetic alloy with the compensation point at $T = 293$ K (considered to be 2 K below room temperature). Figure 13 shows the total energy change ΔE_T that

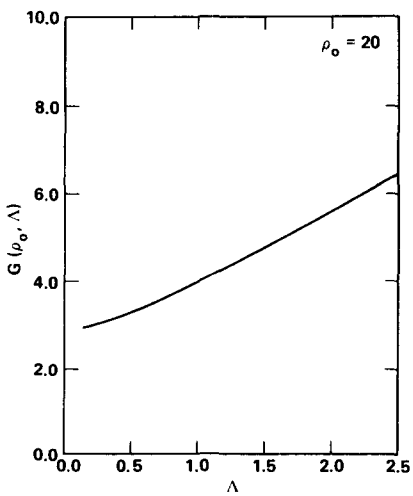

FIG. 9. Plot of $G(\rho_0,\Lambda)$ vs Λ for $\rho_0 = 20$.

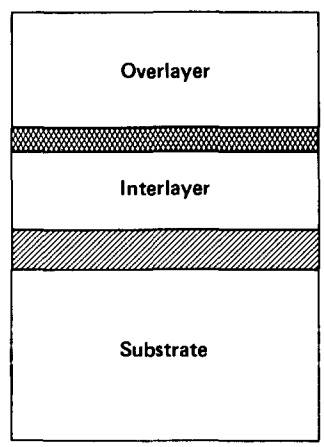

FIG. 10. A schematic representation of the quadrilayer configuration, showing the reflector (hatched), intermediate layer, magnetic film (cross hatched), and overlayer.

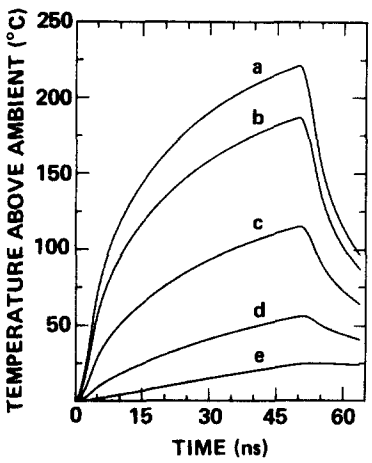

FIG. 11. Increase of temperature versus time at radii of (a) 0, (b) 250, (c) 500, (d) 750, and (e) 1000 nm that occurs in the magnetic film of a quadrilayer medium. The quadrilayer consists of a 50-nm-thick aluminum layer, an 80-nm-thick quartz intermediate layer, a 15-nm-thick magnetic metal and a 120-nm-thick quartz overlayer. The thermal and optical parameters are given in Ref. 3.

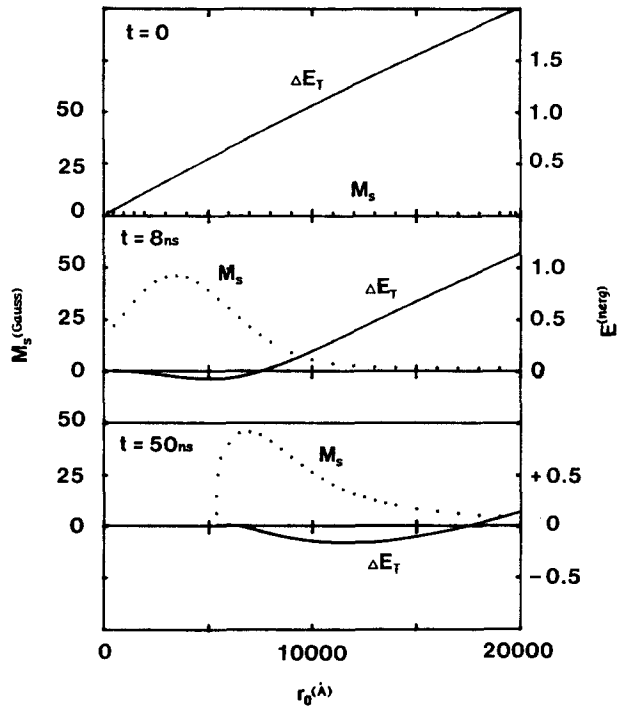

FIG. 13. Net magnetic energy variation (ΔE_T) produced on formation of a domain with radius r_0 in the quadrilayer described in Fig. 11. The dotted curves represent the saturation magnetization (M_s) at each stage. Curves for three instants during the heating period are shown (a) $t = 0$, (b) $t = 8$ ns, (c) $t = 50$ ns.

is produced on formation of a domain of radius r_0 at different stages of the heating process. At $t = 0$, before the laser is turned on, the energy is an increasing function of r_0, and therefore no reversed domain of any radius can be formed. At $t = 8$ ns, however, there is a minimum of energy around $r_0 = 5000$ Å. Whether or not the nucleation begins at this stage depends on the coercivity around $r = 0$, but from energy considerations alone, it is a possibility. At $t = 50$ ns, the end of the heating period, points at $r_0 \leqslant 5200$ Å above the Curie point, and the minimum of energy has moved to $r_0 = 12000$ Å. In this case, whether or not the domain boundary reaches this minimum depends on the wall coercivity and its temperature dependence. The derivative of E_T with respect to r is a measure of the strength of forces acting on the wall, and if the wall is to proceed with its expansion beyond a certain point, these forces must overcome the wall coercivity at that point.

The relative importance of the different contributions to the total energy can be seen in Fig. 14, which shows them at $t = 50$ ns, but the results are typical of all other stages for the magnetic characteristics of the film chosen. It is seen that the self-energy ΔE_M is much smaller than the other terms. For materials with different magnetic characteristics, of

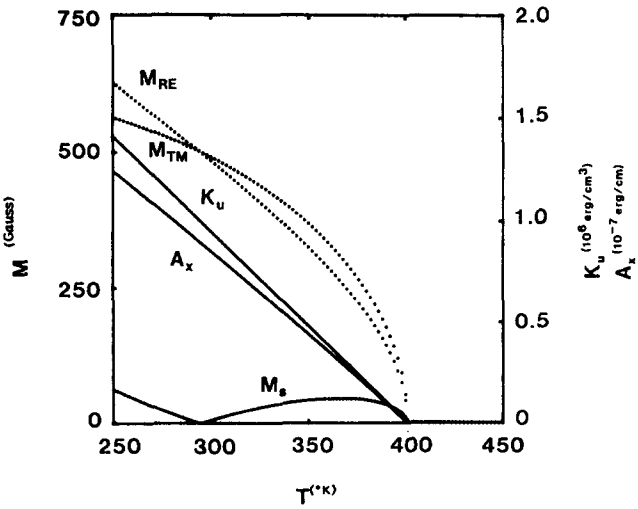

FIG. 12. Mean-field model magnetization of a ferrimagnetic alloy with compensation point around room temperature. Temperature dependence of the exchange stiffness constant A_x and the anisotropy energy constant K_u are also shown.

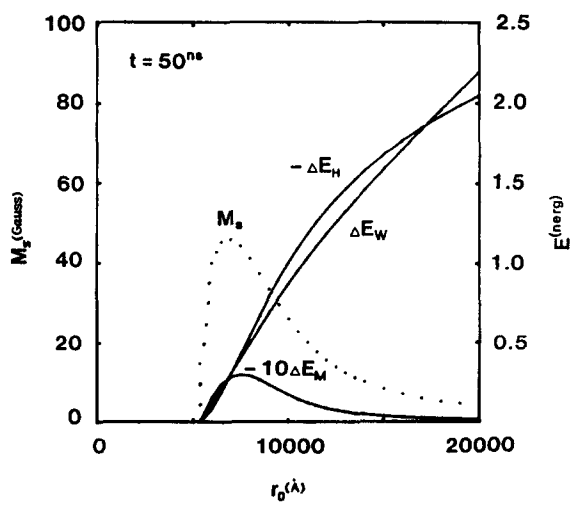

FIG. 14. Individual contributions to the total energy as a function of domain radius r_0 at $t = 50$ ns. $\Delta E_W = \Delta E_K + \Delta E_X$ is the wall energy, ΔE_H is the external field energy ($H_{ext} = 400$ Oe), and ΔE_M is the self-magnetic energy.

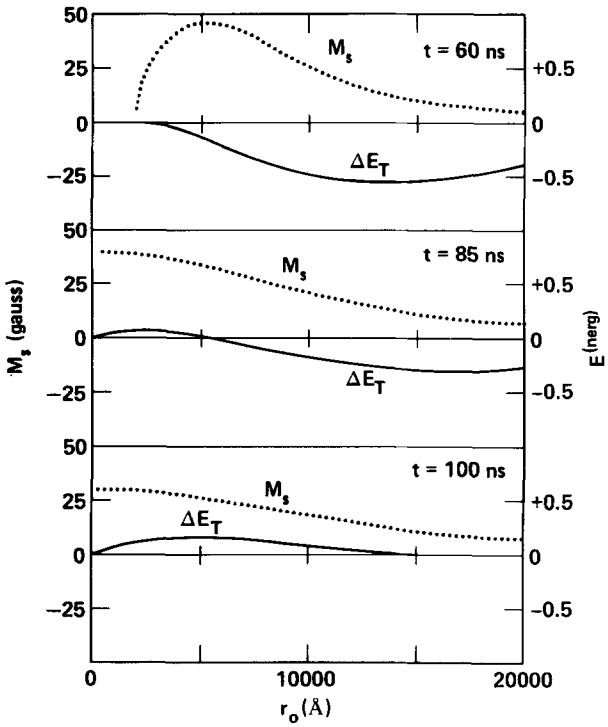

FIG. 15. Same as Fig. 13 but during the cooling period (a) $t = 60$ ns, (b) $t = 85$ ns, (c) $t = 100$ ns.

course, this balance could be different. Interestingly, the domain wall parameter λ remains very close to $(A/K_u)^{1/2}$ at all radii calculated and is not very sensitive to temperature, being about 30 ± 1 Å in the whole temperature range.

A set of ΔE_T curves for the cooling period is shown in Fig. 15. It is seen that depending on the position of the wall at a given instant, the forces acting on the domain wall can be expansive or contractive. It is interesting, however, to note that just after the laser is turned off, when coercivities are low and the wall is between the center of the beam and the radius of minimum energy, the forces tend to be expansive and prevent the written spot from collapsing. This behavior can be seen in the curves for $t = 60$ and 85 ns, and to a smaller extent even at $t = 100$ ns. By the time the temperature drops back to the room temperature, the coercivities have increased drastically, and despite the presence of contractive forces there is no longer any danger of collapse.

The variations of domain-formation energy during a writing cycle that we have described in this section are characteristic of films with room temperature compensation points under reasonable writing conditions. More extensive results for other situations will be reported in the future.

V. CONCLUDING REMARKS

In the example of Sec. IV, the demagnetizing energy was found to be negligible at all stages of the recording process, and the relationship between external field energy and domain wall energy determined the behavior of the curves. If the film thickness increases, however, we can no longer neglect the demagnetizing energy. For the ferrimagnetic material in the calculations, the critical thickness is around 1000 Å. The demagnetizing effects are, in general, in favor of domain formation and therefore large values of demagnetizing energy trnaslate into deeper and/or broader minima for the curves of Fig. 13. One advantage of having a large demagnetizing energy is that recording can be achieved with smaller external fields. Another advantage is that the stability of recorded information becomes less sensitive to the temperature variations in the environment. For example, if the compensation point of the recording medium is at room temperature, in the absence of external fields, the domain walls are subject to contractive forces that tend to reduce the domain size and thereby the domain wall energy. These forces are countered by coercivity and vary as a result of deviation of the ambient temperature from the compensation point. The magnetization, however, increases as a result of such deviations, and if the demagnetizing energy is sufficiently large, it can help reduce the contractive pressures and thus stabilize the domains.

Another situation where the demagnetizing energy may not be neglected occurs when the compensation point of the material is well below the Curie temperature. This could be the case for the material used in our example if the percentage of terbium in the alloy is slightly reduced. While the Curie point of the new material remains essentially unchanged, its compensation point drops substantially. The saturation magnetization thus attains larger values in the temperature range between the room temperature and the Curie point, and as a result, the demagnetizing energy will take a more active role in the process of domain formation. It should be remembered, however, that the new material also has a larger magnetization at room temperature, and the recording field, H_{ext}, may have to be reduced in order to avoid the destabilization of the medium during recording.

Similar considerations apply to the process of erasure. If the demagnetizing energy is negligible, it may be possible to erase the recorded spots without an external field or in the presence of a small reverse field simply by raising the local temperature until the coercivity drops below the contractive forces that act on the domain wall. If the demagnetizing energy is large, however, we will have to use an appreciable external field in the reverse direction together with local heating in order to achieve erasure. The erasure process in this case is likely to be a combination of two processes: nucleation of a new domain within the recorded spot and the destabilization and contraction of the recorded spot itself. If the reverse field is not large enough, the process could lead to partial erasure and the creation of ring-like domains.

[1] B. G. Huth, IBM J. Res. Dev. **18**, 100 (1974).
[2] M. Mansuripur, G. A. N. Connell, and J. W. Goodman, J. Appl. Phys. **53**, 4485 (1982).
[3] M. Mansuripur, G. A. N. Connell, and J. W. Goodman, SPIE Proc. **329**, 215 (1982).
[4] A. H. Eschenfelder, *Magnetic Bubble Technology* (Springer, New York, 1980), pp. 28–30.
[5] A. H. Morrish, *The Physical Principles of Magnetism* (Wiley, New York, 1965), pp. 11–15.
[6] A. A. Thiele, Bell Syst. Tech. J. **48**, 3287 (1969).
[7] M. Mansuripur, G. A. N. Connell, and J. W. Goodman, Appl. Opt. **21**, 1106 (1982).
[8] N. Heiman, K. Lee, and R. I. Potter, AIP Conf. Proc. **29**, 130 (1975).
[9] A. Gangulee and R. Kobliska, J. Appl. Phys. **49**, 4896 (1978).
[10] T. Mizoguchi and G. Cargill, J. Appl. Phys. **50**, 3570 (1979).